Terahertz Radiation from Magnetic Excitations in Diluted Magnetic Semiconductors

R. Rungsawang,[1] F. Perez,[2,*] D. Oustinov,[1] J. Gómez,[2,†] V. Kolkovsky,[3] G. Karczewski,[3] T. Wojtowicz,[3] J. Madéo,[1] N. Jukam,[1] S. Dhillon,[1] and J. Tignon[1]

[1]*Laboratoire Pierre Aigrain, Ecole Normale Supérieure, CNRS (UMR 8551), Université Pierre et Marie Curie, Université D. Diderot, 75231 Paris Cedex 05, France*

[2]*Institut des Nanosciences de Paris, CNRS (UMR7588), Université Paris VI, Paris 75005, France*

[3]*Institute of Physics, Polish Academy of Sciences, 02-668 Warsaw, Poland*

(Received 13 June 2012; revised manuscript received 4 April 2013; published 23 April 2013)

We probed, in the time domain, the THz electromagnetic radiation originating from spins in CdMnTe diluted magnetic semiconductor quantum wells containing high-mobility electron gas. Taking advantage of the efficient Raman generation process, the spin precession was induced by low power near-infrared pulses. We provide a full theoretical first-principles description of spin-wave generation, spin precession, and of emission of THz radiation. Our results open new perspectives for improved control of the direct coupling between spin and an electromagnetic field, e.g., by using semiconductor technology to insert the THz sources in cavities or pillars.

DOI: 10.1103/PhysRevLett.110.177203 PACS numbers: 75.50.Pp, 07.57.Hm, 73.21.Fg, 75.78.Jp

Spin-based sources of THz electromagnetic radiation have recently attracted a great deal of attention, especially since spin waves were proposed to provide radiating sources to transmit or modify logical spin-based information [1]. In this context, direct light emission or absorption from the spin degrees of freedom is at the frontier of novel physics [2]. Until now, however, optically [3–5] or magnetically [6] excited spin waves have been primarily investigated in antiferromagnets such as NiO. It is less obvious to expect similar THz emission from spin excitations in semiconductors, since typical semiconductors are paramagnetic and are limited by much lower concentrations of available spins (by a factor of 10^{-4}), which results in much weaker emitted fields. Even worse, conventional semiconductors are lacking an optical spin mode with a frequency in the THz range. On the other hand, however, semiconductors—and particularly the engineering of nanostructures with high materials quality—offer an excellent laboratory for controlling and studying the coupling of photon modes with the spin degrees of freedom and thus for making advances in the spin-based THz emission.

Here we provide the first steps in the experimental and theoretical exploration of spin-based THz emission from diluted magnetic semiconductor (DMSs) [7,8] quantum wells. In DMSs, the number of available spins is controlled by the concentration x of magnetic ions (e.g., Mn) incorporated into the nonmagnetic host, so as to form crystals as $Ga_{1-x}Mn_xAs$ or $Cd_{1-x}Mn_xTe$. Moreover, spin excitations occur in the form of mixed modes, in which spins of the free band carriers and those of localized magnetic ions oscillate coherently, in phase (acoustic modes) or out of phase (optical modes) [9,10]. The precession frequency of these optical modes typically follows the spin-split (Zeeman) energy of the carriers, Z, which is enhanced by the large exchange interaction with the d-shell electrons of the localized Mn ions. Thus the precession frequency can be adjusted in the THz range both by x and by the DMS exchange integral $N_0\beta$ (for holes) or $N_0\alpha$ (for electrons).

THz transient emission from $Ga_{1-x}Mn_xAs$ in the ferromagnetic state has already been detected by the time domain measurements [11]. However, the spin origin of the radiation was not demonstrated, as the frequency range of the observed transient did not match either the acoustic or optical mode frequencies. We preferentially used a well controlled test-bed DMS system made of a two-dimensional electron gas (2DEG) embedded in a $Cd_{1-x}Mn_xTe$ quantum well (QW), which has been introduced [12–15] as an alternative for magnetic excitation study in DMS. In this *paramagnetic* system, the acoustic and optical spin wave modes have been evidenced by Raman spectroscopy [12–15] and time-domain optical pump-probe experiments [16,17]. Upon application of an external magnetic field $B\mathbf{z}$ parallel to the quantum well plane (see inset of Fig. 1 and Ref. [18]), each paramagnetic Mn atom supports a thermal average spin $\langle I_z(B,T)\rangle$. The spin-split Zeeman energy Z of the QW conduction band is written

$$Z(B,T) = \bar{x}N_0\alpha\langle I_z(B,T)\rangle - |g_e|\mu_B B. \quad (1)$$

In Eq. (1), $N_0\alpha = -0.22$ eV [19], $\bar{x}$ is the effective Mn concentration (for low x, $\bar{x} \simeq x$), and $g_e = -1.64$ is the electron Landé factor in CdMnTe ($\mu_B > 0$).

In our experiment, the spin-polarized 2DEGs reside in each of 20 QWs within a $Cd_{1-x}Mn_xTe$ multi-quantum-well structure [18]. The sample exhibit well resolved quantum Hall plateaus and Shubnikov–de Haas oscillations. 2DEG sheet densities n_{2D} and mobilities were found to be 5×10^{11} cm^{-2} and 2.4×10^4 cm^2/V s. The Mn concentration, as determined from Raman measurements [14], is $x = 1.75\%$, which implies that Z can be as high as 6.7 meV

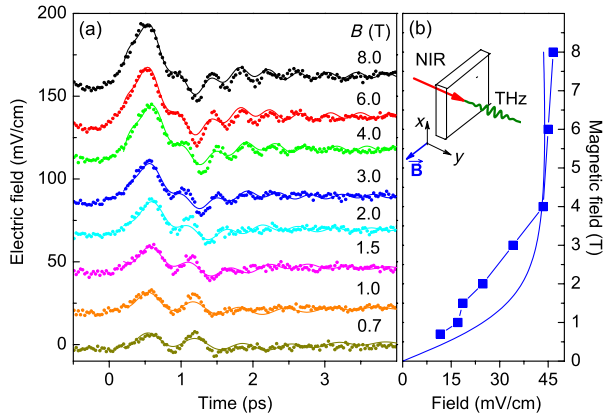

FIG. 1 (color online). (a) Time-dependent radiated fields for various magnetic fields (B). A vertical offset is added for clarity. Fitted sinusoids are superposed. (b) (squares) Amplitude of the transient oscillation extracted from (a), as a function of the magnetic field. (line) Radiated amplitude calculated for one quantum well (see text). (Inset) Sketch of the experiment: a near-infrared (NIR) pulse (100 fs) with circular polarization is focused, with normal incidence, on the QW structure. The sample is immersed in a bath of superfluid helium inside a split-coil magnet with a static field B up to 8 T applied along the quantum well plane (parallel to the z direction). The THz transient electric field is collected along the z direction [18].

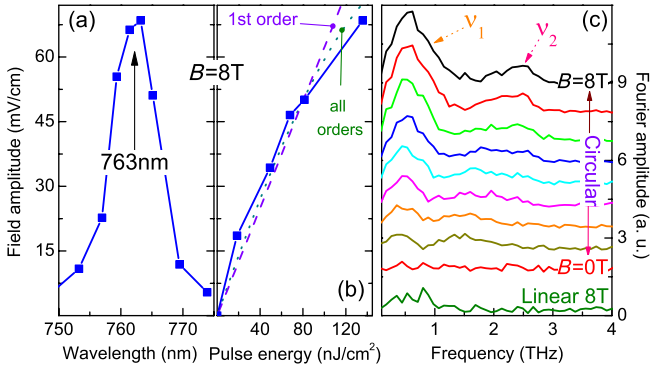

FIG. 2 (color online). (a) Transient electric field amplitude as a function of central wavelength of the pulse. The pulse energy was 136 nJ/cm^2. (b) Variation of the detected radiated amplitude (squares) with the pulse energy and comparison with the calculations carried to first order with Eqs. (3) and (4) and to all orders [18]. (c) Fourier transforms of the electric field transients shown in Fig. 1(a). Two peaks, labeled ν_1 and ν_2, are identified. The bottom curve is the result of linearly polarized excitation at $B = 8$ T. All the curves above, from $B = 0$ T to $B = 8$ T, are obtained with a circular pulse.

($\simeq 1.6$ THz) for $B = 8$ T. In this case the 2DEG becomes highly spin polarized with a spin polarization degree $\zeta = (n_\uparrow - n_\downarrow)/(n_\uparrow + n_\downarrow) \simeq -Z/2E_F \simeq 40\%$ (E_F is the Fermi energy). A circularly polarized near-infrared femtosecond pulse propagating perpendicularly to the quantum well plane (see inset of Fig. 1 and Ref. [18]) exchanges angular momentum with the electron spins and the Mn spins through a Raman generation process thanks to strong spin-orbit interaction in the valence states [20,21]. A collective spin precession starts and within the relaxation time, the spin oscillation radiates an electromagnetic field which is probed by electro-optic sampling. In Fig. 1(a), we have plotted for various static magnetic fields, the transient electric field radiated from the sample excited by an optical pulse centered at 763 nm. The electro-optic sampling detection was set to be sensitive to the electric field component *parallel to the static magnetic field axis* (**z** axis). A transient, well resolved oscillation of the emitted field is observed. The amplitude of the electric field oscillation saturates with the external magnetic field as expected [see Fig. 1(b) and text below]. The emission was measured with an energy per pulse $E_P \simeq 70$ nJ/cm^2, which is orders of magnitude smaller than that used for $Ga_{1-x}Mn_xAs$ in Ref. [11] (400 μJ/cm^2) or for NiO in Ref. [22] (20 mJ/cm^2). The power requirements in this work are strongly reduced by the strong spin-orbit interaction occurring in valence states and the sharpness of the optical resonance involved in the Raman generation mechanism. The latter is assured by the recent progress of MBE growth of II–VI semiconductor heterostructures [23].

Illustration of the resonance is given in Fig. 2(a), where for a fixed magnetic field, we tuned the central wavelength λ_0 of the optical pulse across the lowest 2DEG's optical resonance positioned at 763 nm (as determined by cw optical measurements). The amplitude of the radiated oscillation is maximum at 763 nm. This is the first evidence that the emission originates from 2DEG electrons and not from the CdTe buffer or from the GaAs substrate.

The spin origin of the radiation is inferred from Fig. 2(c), where the Fourier-transforms of the detected field transients [shown in Fig. 1(a)] are plotted for circularly and linearly polarized optical pulses in the presence or absence of the magnetic field. As clearly seen, the radiation is detected only when the magnetic field is switched on and when the optical pulse is circularly polarized. This reflects perfectly the symmetry of the inverse Faraday effect [24–26] in a cubic crystal: a circularly polarized pulse exchange a transient magnetic moment along the propagation direction while a linearly polarized pulse has no magnetic effect, but couples to charge excitations only [20]. In addition, in absence of external magnetic field, the out-of-phase spin wave disappears. These observations also demonstrate that the detected radiation cannot be related to a magnetic field enhancement of a radiation originating from charge excitations as described in Ref. [27]. Indeed, the pulse, normally incident and focused on a 1 mm diameter spot, can induce a charge motion only perpendicular to the quantum well plane, and the Lorentz force is unable to induce a dipole along the magnetic field axis (**z** axis), which is the detected radiation polarization.

We confirm the spin origin by providing a quantitative treatment of the amplitude of the radiation and the frequencies present in the generated THz transient and

demonstrate that it supports the data. The impulsive optical electromagnetic field, circularly polarized in the plane ($\mathbf{x}$, $\mathbf{z}$) of the sample, couples to the crystal through the Hamiltonian, $\hat{H}(t) = -e\mathbf{A}(t)\cdot\hat{\mathbf{p}}/m^* = \int \tilde{H}_\omega e^{i\omega t} d\omega$, where $\mathbf{A}(t)$ is the time-dependent vector potential. Before the pulse excites the sample, the crystal is in its equilibrium state $|i\rangle$ where electron and Mn spins are antiparallel to the magnetic field. The macroscopic electron spin $\hat{\mathbf{S}} = \sum_j \hat{\mathbf{s}}_j$ is then $\langle i|\hat{S}_z|i\rangle = S_{zi} = \frac{1}{2} n_{2D} L^2 \zeta$, where L^2 is the illuminated QW surface. The macroscopic Mn spin $\hat{\mathbf{M}} = \sum_j \hat{\mathbf{I}}_j$ has the equilibrium value $\langle i|\hat{M}_z|i\rangle = M_{zi} = xN_0\langle I_z(B,T)\rangle wL^2$, where w is the QW thickness. After its action, through the Raman process, the pulse leaves the system in the state [18,21]

$$|\Psi(t)\rangle = c_i e^{-i\omega_i t}|i\rangle + \sum_m c_m e^{-i\omega_m t}|m\rangle, \tag{2}$$

where $|m\rangle$ are excited quantum states with eigenpulsation ω_m, and c_m is written (to lowest order in the field [18]),

$$c_m = i\frac{\pi}{\hbar^2}\int \sum_n \frac{\langle m|\tilde{H}_{\omega-\omega_{mi}}|n\rangle\langle n|\tilde{H}^*_\omega|i\rangle}{\omega_{ni} - \omega + i\eta_n} d\omega. \tag{3}$$

In Eq. (3), $|n\rangle$ are intermediate states, η_n is their decay rate, and $\omega_{mi} = \omega_m - \omega_i$. Note that the optical pulse resonates with the crystal transition when $\omega \simeq \omega_n - \omega_i$ over a range given typically by η_n. A coherence between $|i\rangle$ and a spin-wave state $|f\rangle$ will be driven, if the pulse spectrum contains two photons separated by ω_{fi} and if these two photons can together transfer magnetic momentum. For the latter, the spin mixture in the hole state involved in the interband electron-hole-pair intermediate state $|n\rangle$ is essential [18,20,21]. The cubic symmetry of the CdTe crystal makes the Raman process obey the general symmetry of the inverse Faraday effect [25,26]. It results [18] in $c_f = i\int \chi_f(\omega)\langle f|\hat{\mathbf{S}}\cdot\mathbf{A}_{\omega-\omega_{fi}}\times\mathbf{A}^*_\omega|i\rangle d\omega$, where $\chi_f(\omega)$ is a scalar. Therefore, the circularly polarized pulse couples to the spin degrees of freedom as an effective magnetic field proportional to $\mathbf{A}_{\omega-\omega_{fi}}\times\mathbf{A}^*_\omega$, which is vanishing for a linearly polarized pulse but directed along the propagation direction $\mathbf{y}$ for a circular pulse. Thus, our circular pulse induces an out-of-equilibrium magnetization and leaves the system in a state such that the average Mn and electron spins are respectively $\mathbf{M}(t=0) = (0, M_{y0}, M_{z0})$ and $\mathbf{S}(t=0) = (0, S_{y0}, S_{z0})$ ($\mathbf{M}(t) = \langle\Psi(t)|\hat{\mathbf{M}}|\Psi(t)\rangle$). Both macroscopic spins will further experience a spontaneous precession with a relaxation towards their equilibrium states.

In a semiclassical picture, the spin magnetization is associated with a surface current density carried by each quantum well, $\mathbf{i}_s = g_e\mu_B\mathbf{S}(t)\times\mathbf{y}/wL^2$, where $\mathbf{S}(t) = \langle\Psi(t)|\hat{\mathbf{S}}|\Psi(t)\rangle$. Continuity relations of the electromagnetic field at the QW interface lead to the radiated field from each QW after transmission in the air,

$$\mathbf{e}_R(t) = \frac{2c\mu_0}{1+n}\frac{g_e\mu_B}{wL^2} S_x(t)\mathbf{z}, \tag{4}$$

where n is the refraction index of the substrate. Therefore, the radiated field is polarized parallel to the z axis, consistent with the experimental observations. Its instantaneous value is proportional to the transverse component $S_x(t)$, and its amplitude is proportional to the number of spins, thus, to the spin-polarization degree ζ that saturates with B as the Zeeman energy of Eq. (1) does. As shown in Fig. 1(b), the measured amplitude of the radiated field reproduces this behavior. The transverse component of the spin is induced by the optical pulse. Consequently, the radiated amplitude is maximum for a pulse energy for which the spins are totally tilted out of their equilibrium axis. Fig. 2(b) shows the trend of a saturation of the emitted amplitude when the energy per pulse is further increased from $\simeq 80$ nJ/cm^2. Thus, the emitted amplitude naturally departs from the calculations of Eqs. (3) and (4) valid to lowest order in the optical field. A better agreement in the high-energy regime has been obtained when going beyond this approximation by resolving the intrapulse spin dynamics to all orders [18]. A similar nonlinear behavior has been found in Ref. [28].

The frequency analysis shown in Fig. 2(c) reveals two main frequencies, ν_1 and ν_2. The two frequencies present in the transients are extracted by a linear prediction algorithm [18] and plotted in Fig. 3(a). The fitted signal is superposed in Fig. 1(a). In Fig. 3(a), the two frequencies ν_1 and ν_2 are compared with the precession frequency of the optical spin mode determined by Raman spectroscopy (blue dots) [14]. The latter matches $Z(B,T)/h$ (blue curve), where Z is given in Eq. (1). However, although both ν_1 and ν_2 frequencies exhibit a similar magnetic field dependence, they are not directly associated with $Z(B,T)/h$ and appear as two frequencies almost symmetrically split from $Z(B,T)/h$.

The transient at $B = 8$ T shows that the probed spin component $S_x(t)$ experiences quick changes of its phase. This strongly suggests that its precession axis evolves in time. The phenomenon is similar to a magnetic resonance, where a magnetic field $\mathbf{b}_1$ oscillates transversally to the polarizing magnetic field $B\mathbf{z}$. Here, the oscillating field is the strong exchange field of the Mn spins, which acts as a torque $\alpha\mathbf{S}\times\mathbf{M}$. $\mathbf{M}(t)$ precesses around the $\mathbf{z}$ axis at $\omega_{\mathrm{Mn}} = g_{\mathrm{Mn}}\mu_B B/\hbar$ [see lowest green line in Fig. 3(a)], since we can neglect the action of the exchange field from the electrons [18]. Due to the transverse oscillation of the Mn-exchange field, the z component of the electron spin $S_z(t)$ oscillates at the Rabi pulsation,

$$\Omega = \frac{1}{\hbar}\sqrt{(\alpha M_{y0})^2 + (\hbar\omega_{\mathrm{Mn}} - \alpha M_{z0} + |g_e|\mu_B B)^2}, \tag{5}$$

and the transverse component $S_x(t)$ has a motion composed of three sinusoids at pulsations ω_{Mn} and $\Omega \pm \omega_{\mathrm{Mn}}$. The corresponding three frequencies are plotted in Fig. 3(a)

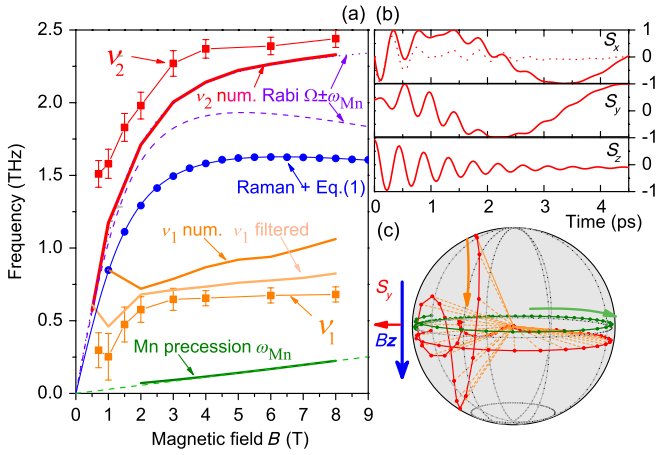

FIG. 3 (color online). (a) ν_1 (orange squares) and ν_2 (red squares) are the frequencies present in the transient radiated field. *Raman* (blue dots) is the optical spin mode frequency determined by Raman measurements. The Raman determination is fitted with Eq. (1) for $x = 1.75\%$, $T = 2.34$ K, and $g_e = -1.64$ (blue curve). *Rabi* are the frequencies given by Eq. (5) (dashed and dotted purple curves). ω_{Mn} are the Mn precession frequencies from theory (dashed green curve) and simulations (solid green curve). ν_1 *num.*, ν_2 *num.*, and ν_1 *filtered* are frequencies deduced from the simulated $S_x(t)$ before (red and orange curves) and after (light orange curve) filtering. (b) Normalized $S_x(t)$, $S_y(t)$, and $S_z(t)$ as calculated from Eq. (6) for $B = 8$ T. The dashed $S_x(t)$ curve is obtained after numerical high-pass filtering. (c) $\mathbf{S}(t)$ (red) and $\mathbf{M}(t)$ (green) are the spin trajectories. The external magnetic field $B\mathbf{z}$ is vertical downward. After the pulse, electrons spins have been tilted in the y direction with normalized $S_{y0} = 0.4$, while the Mn spins are parallel to the y axis. The latter precess slowly in the (xy) plane as indicated by the green arrow. Electron spins try to precess around the Mn spin axis as indicated by the orange arrow. After the relaxation of their transverse components (respective to the rotating Mn precession axis), the electron spins follow the slow Mn precession.

(green dashed and purple dotted and dashed curves). $\Omega + \omega_{Mn}$ matches ν_2 within 10% when setting $M_{z0} = 0$, i.e., when assuming that the Mn spins have been tilted totally out of the plane after the pulse. However, ν_1 does not match $\Omega - \omega_{Mn}$.

In order to understand the discrepancy concerning ν_1, we solved numerically the set of coupled equations of motion for $\mathbf{S}(t)$ and $\mathbf{M}(t)$ (see Ref. [18] for details),

$$\frac{d\mathbf{S}}{dt} = |g_e|\tilde{\mu}_B B\mathbf{S}\times\mathbf{z} + \tilde{\alpha}\mathbf{S}\times\mathbf{M} - \frac{\alpha_e}{|S_{zi}|}\mathbf{S}\times\frac{d\mathbf{S}}{dt}, \quad (6)$$

where $\tilde{\mu}_B = \mu_B/\hbar$ and $\tilde{\alpha} = \alpha/wL^2/\hbar$, α_e is a Gilbert damping parameter. $\mathbf{M}(t)$ is driven by a similar equation [18]. The time evolution of $\mathbf{S}(t)$ and spin trajectories are plotted in Figs. 3(b) and 3(c), respectively. To account for the fast electron spin relaxation rate (3 ps), α_e was set to 0.07, while for the slower Mn relaxation, we used $\alpha_{Mn} = 0.01$. From Fig. 3(c), we see that the electron spins try to precess around the oscillating $\mathbf{M}(t)$ axis. The damping relaxes its components transverse to the oscillating axis; hence, after 3 ps, $\mathbf{S}(t)$ follows $\mathbf{M}(t)$.

A detailed frequency analysis of the simulated $S_x(t)$ results in three characteristic frequencies. The highest frequency [ν_2 *num.*, solid red curve in Fig. 3(a)] is in very good agreement with $\Omega + \omega_{Mn}$ and, hence, ν_2; the lowest frequency corresponds to ω_{Mn}, and the intermediate one (ν_1 *num.*, solid orange curve) is close to ν_1 as shown in Fig. 3(a). The ω_{Mn} pulsation is not seen in the transient of Fig. 2(a) because the detection process of the THz field acts as a sharp high pass-filter with cutoff frequency around 0.3 THz. To account for this, we have filtered the simulated $S_x(t)$ with a numerical high-pass filter [18]. The filtered trajectory of $S_x(t)$ is plotted in Fig. 3(b). The filtering has a negligible effect on ν_2 *num.*, but slightly shifts ν_1 *num.* to lower values (ν_1 *filtered*, solid light orange curve), increasing its agreement with ν_1. To summarize, the identification of frequencies observed in the transient is supported by the theory within a 10% quantitative agreement, when taking into consideration the nonlinear coupled spin dynamics between the electrons and the Mn ions. The time dependent coupling between these two systems splits the observed frequencies from Z/h. This mechanism explains in addition the difference with the Raman determination of the precession modes. Raman probes spin fluctuations; therefore, the Mn spins are negligibly disturbed such that $M_{y0} \simeq 0$ and electrons are sensitive to a static exchange magnetic field aligned with the z axis.

In conclusion, we have measured THz transient fields radiated from optically generated spin-wave excitations in DMS multiple quantum wells. The radiation is polarized parallel to the static magnetic field axis and appears only with a circular polarized pulse. Thus, its origin cannot be attributed to charge excitations. The spin-wave origin of the emitted field is supported by first-principles theoretical analysis of all aspects of the experiment, including the generation mechanism, spin dynamics, and properties of emitted radiation. Hence, we provide evidence that DMS quantum wells constitute a highly promising test bed for deeper investigations in the basic issues of spin-based THz emission, such as addressing the intrinsic spin precession decay caused by the radiation [29] or manipulating the coupling between spin and radiation at the quantum level, e.g., by inserting such DMS quantum wells into cavities [30,31].

F. P. thanks L. Thevenard for detailed discussions on GaMnAs. Authors thank M. Wiater for expert technical assistance in the MBE growth. This research has been supported by the funding of CNANO IdF (SPINWAVDYN), ANR(GOSPININFO), the research program of Mairie de Paris, the NSC (Poland) Grant No. 2012/06/A/ST3/00247, and the ERDF European Union Grant No. POIG.01.01.02-00-008/08.

*Corresponding author.
florent.perez@insp.jussieu.fr
†Present address: Centro Atómico Bariloche, Bariloche, Argentina.

[1] S. A. Wolf, A. Y. Chtchelkanova, and D. M. Treger, IBM J. Res. Dev. **50**, 101 (2006).
[2] J. Kono, Nat. Photonics **5**, 5 (2011).
[3] E. Beaurepaire, G. M. Turner, S. M. Harrel, M. C. Beard, J.-Y. Bigot, and C. A. Schmuttenmaer, Appl. Phys. Lett. **84**, 3465 (2004).
[4] K. Yamaguchi, M. Nakajima, and T. Suemoto, Phys. Rev. Lett. **105**, 237201 (2010).
[5] J. Nishitani, T. Nagashima, and M. Hangyo, Phys. Rev. B **85**, 174439 (2012).
[6] T. Kampfrath, A. Sell, G. Klatt, A. Pashkin, S. Mährlein, T. Dekorsy, M. Wolf, M. Fiebig, A. Leitenstorfer, and R. Huber, Nat. Photonics **5**, 31 (2011).
[7] H. Ohno, Science **281**, 951 (1998).
[8] J. K. Furdyna, J. Appl. Phys. **64**, R29 (1988).
[9] F. Perez, J. Cibert, M. Vladimirova, and D. Scalbert, Phys. Rev. B **83**, 075311 (2011).
[10] J. König, H. H. Lin, and A. H. MacDonald, Phys. Rev. Lett. **84**, 5628 (2000).
[11] J. B. Héroux, Y. Ino, M. Kuwata-Gonokami, Y. Hashimoto, and S. Katsumoto, Appl. Phys. Lett. **88**, 221110 (2006).
[12] F. J. Teran, M. Potemski, D. Maude, D. Plantier, A. Hassan, A. Sachrajda, Z. Wilamowski, J. Jaroszynski, T. Wojtowicz, and G. Karczewski, Phys. Rev. Lett. **91**, 077201 (2003).
[13] B. Jusserand, F. Perez, D. Richards, G. Karczewski, T. Wojtowicz, C. Testelin, D. Wolverson, and J. Davies, Phys. Rev. Lett. **91**, 086802 (2003).
[14] F. Perez, C. Aku-leh, D. Richards, B. Jusserand, L. Smith, D. Wolverson, and G. Karczewski, Phys. Rev. Lett. **99**, 026403 (2007).
[15] C. Aku-Leh, F. Perez, B. Jusserand, D. Richards, and G. Karczewski, Phys. Rev. B **83**, 035323 (2011).
[16] M. Vladimirova, S. Cronenberger, P. Barate, D. Scalbert, F. Teran, and A. Dmitriev, Phys. Rev. B **78**, 081305 (2008).
[17] P. W. Jacobs, F. Perez, C. Aku-leh, R. Merlin, and G. Karzewski, AIP Conf. Proc. **1199**, 423 (2010).
[18] See Supplemental Material at http://link.aps.org/supplemental/10.1103/PhysRevLett.110.177203 for details on the sample structure, the THz setup, and the intermediate calculations of equations present in the text.
[19] J. Gaj, R. Planel, and G. Fishman, Solid State Commun. **29**, 435 (1979).
[20] J. M. Bao, L. N. Pfeiffer, K. W. West, and R. Merlin, Phys. Rev. Lett. **92**, 236601 (2004).
[21] D. Popova, A. Bringer, and S. Blügel, Phys. Rev. B **84**, 214421 (2011).
[22] J. Nishitani, K. Kozuki, T. Nagashima, and M. Hangyo, Appl. Phys. Lett. **96**, 221906 (2010).
[23] B. A. Piot, J. Kunc, M. Potemski, D. K. Maude, C. Betthausen, A. Vogl, D. Weiss, G. Karczewski, and T. Wojtowicz, Phys. Rev. B **82**, 081307 (2010).
[24] A. V. Kimel, A. Kirilyuk, P. A. Usachev, R. V. Pisarev, A. M. Balbashov, and Th. Rasing, Nature (London) **435**, 655 (2005).
[25] P. S. Pershan, J. P. Van der Ziel, and L. D. Malmstrom, Phys. Rev. **143**, 574 (1966).
[26] T. Higuchi, N. Kanda, H. Tamaru, and M. Kuwata-Gonokami, Phys. Rev. Lett. **106**, 047401 (2011).
[27] C. Weiss, R. Wallenstein, and R. Beigang, Appl. Phys. Lett. **77**, 4160 (2000).
[28] S. G. Carter, Z. Chen, and S. T. Cundiff, Phys. Rev. B **76**, 201308 (2007).
[29] M. C. Hickey and J. S. Moodera, Phys. Rev. Lett. **102**, 137601 (2009).
[30] Ö. O. Soykal and M. E. Flatté, Phys. Rev. Lett. **104**, 077202 (2010).
[31] J. Li, T. Higuchi, N. Kanda, K. Konishi, S. G. Tikhodeev, and M. Kuwata-Gonokami, Opt. Express **19**, 22 550 (2011).